Geophys. J. Int. (1996) **126**, 525–544

Observability of the isotropic component of a moment tensor

Hitoshi Kawakatsu
Earthquake Research Institute, University of Tokyo, Tokyo 113, *Japan*

Accepted 1996 March 29. Received 1996 March 27; in original form 1995 August 24

SUMMARY

The observability of the isotropic component of a general moment tensor is investigated by carefully examining its resolvability from the other components. It is shown that the portion of seismograms between the first *P*-wave arrival and just before the arrival of the first surface wavetrain, which contains many different body-wave phases, can be used to constrain the isotropic component of deep earthquakes. CMT inversion using this portion of the seismogram for major deep earthquakes has revealed that there is no significant isotropic component for deep earthquakes. This conclusion contradicts some earlier studies, for example Dziewonski & Gilbert (1974), who found significant isotropic components of deep earthquakes by analysing normal-mode data. It is shown that the isotropic component of deep earthquakes cannot be resolved independently from the vertical CLVD component of the moment tensor by analysing the type of normal-mode data above 2 mHz that previous researchers used. At the same time, however, the possibility of resolving the isotropic component using normal-mode data below 2 mHz is suggested.

Key words: body waves, deep focus earthquakes, earthquake-source mechanism, global seismology, normal modes, surface waves.

INTRODUCTION

The seismic moment tensor, which describes the overall geometry and size of an earthquake, was first introduced by Gilbert (1970) as a generalization of the stress drop associated with an earthquake. Backus & Mulcahy (1976) later gave a sound theoretical basis for the moment tensor description of earthquake source mechanisms by introducing the idea of 'stress glut', and suggested that it could describe any 'indigenous source' within the Earth. Although there are some indigenous sources that cannot be described by the moment tensor (e.g. Kanamori & Given 1981; Kawakatsu 1989; Takei & Kumazawa 1994), the moment tensor is still the most general description of any indigenous source resulting from the release of strain energy (Takei & Kumazawa 1995). Because of this generality, together with the linear relationship of the moment tensor to the seismic wavefield, the determination of the moment tensor from seismic data (i.e. moment tensor inversion) has become the most common approach to describing earthquake source mechanisms. Owing to the great advances in global seismology in the last 20 years or so, moment tensor inversion for the world's major earthquakes has now become a routine matter (e.g. Dziewonski, Franzen & Woodhouse 1984; Ekström 1993; Sipkin 1994; Kawakatsu 1995).

It is, however, well known that the six components of the moment tensor are not equally observable. For example, Kanamori & Given (1981) showed that the $M_{r\theta}$ and $M_{r\phi}$ components of a shallow (<10 km) earthquake cannot be determined from long-period surface-wave data, and it is often necessary to use other information (e.g. first-motion polarities) to constrain those components. The general difficulty of constraining the isotropic part of the moment tensor, which is the subject of this paper, has also been recognized; in most applications of moment tensor inversion the diagonal component is constrained to be zero (e.g. Dziewonski *et al.* 1981; Kanamori & Given 1981), even though it is not necessarily known that there is no isotropic component.

Because of its important implications for the origin of deep earthquakes, whether or not deep earthquakes have a significant isotropic component has been the subject of great debate. Dziewonski & Gilbert (1974) and Gilbert & Dziewonski (1975) (hereafter referred to as DG74 and GD75, respectively), in their pioneering work on the Earth's normal modes and moment tensor inversion, reported that they observed significant implosive isotropic components for two large deep earthquakes. Since then, many researchers have attempted to either prove or disprove their result (e.g. Geller 1974; Hart & Kanamori 1975; Kennett & Simons 1976; Mendiguren & Aki 1978; Okal & Geller 1979), but no definitive conclusion seems to have emerged. More recent attempts to observe the isotropic component of deep earthquakes do not yet seem to have ended this debate (e.g. Silver & Jordan 1982; Riedesel 1985; Riedesel & Jordan 1989; Vasco & Johnson 1989).

Table 1. Body and surface wave radiation pattern.

		I	C	$(D, M_{\theta\phi})$	$(M_{r\theta}, M_{r\phi})$
				2ϕ	ϕ
(P)	$\hat{\gamma}\cdot M\cdot\hat{\gamma}$	1	$(1-3\cos^2 i_\xi)/2$	$\sin^2 i_\xi\cdot(\cos 2\phi, \sin 2\phi)$	$\sin 2i_\xi\cdot(\cos\phi, \sin\phi)$
(SV)	$\hat{p}\cdot M\cdot\hat{\gamma}$		$3/4\sin 2i_\xi$	$1/2\sin 2i_\xi\cdot(\cos 2\phi, \sin 2\phi)$	$\cos 2i_\xi\cdot(\cos\phi, \sin\phi)$
(SH)	$\hat{\phi}\cdot M\cdot\hat{\gamma}$			$\sin i_\xi\cdot(-\sin 2\phi, \cos 2\phi)$	$\cos i_\xi\cdot(-\sin\phi, \cos\phi)$
(R)	$\hat{V}_r(\mathbf{r},\omega)$	$N_R^{(1)}$	$1/2S_R^{(1)}$	$-P_R^{(1)}\cdot(\cos 2\phi, \sin 2\phi)$	$iQ_R^{(1)}\cdot(\cos\phi, \sin\phi)$
(G)	$\hat{V}_\phi(\mathbf{r},\omega)$			$P_L^{(1)}\cdot(\sin 2\phi, \cos 2\phi)$	$iQ_L^{(1)}\cdot(-\sin\phi, \cos\phi)$

For notation, refer to Fig. 4.20 of Aki & Richards (1980) for body waves, and to Kanamori & Given (1981) for surface waves. i_ξ and ϕ are the take-off angle and azimuth of rays, respectively.

Reorganization of Diagonal Components

$$(M_{rr}, M_{\theta\theta}, M_{\phi\phi}, M_{r\theta}, M_{r\phi}, M_{\theta\phi}) \rightarrow (I, C, D, M_{r\theta}, M_{r\phi}, M_{\theta\phi})$$

$$I \equiv \tfrac{1}{3}(M_{\theta\theta} + M_{\phi\phi} + M_{rr}) \qquad \text{(Isotropic)}$$

$$C \equiv \tfrac{1}{3}(M_{\theta\theta} + M_{\phi\phi} - 2M_{rr}) = (DV_{\theta\theta} + DV_{\phi\phi}) \qquad \text{(CLVD)}$$

$$D \equiv \tfrac{1}{2}(M_{\theta\theta} - M_{\phi\phi}) = \tfrac{1}{2}(DV_{\theta\theta} - DV_{\phi\phi}) \qquad \text{(Difference)}$$

where

$$DV_{ij} \equiv M_{ij} - I\cdot\delta_{ij} \qquad \text{(Deviatoric)}$$

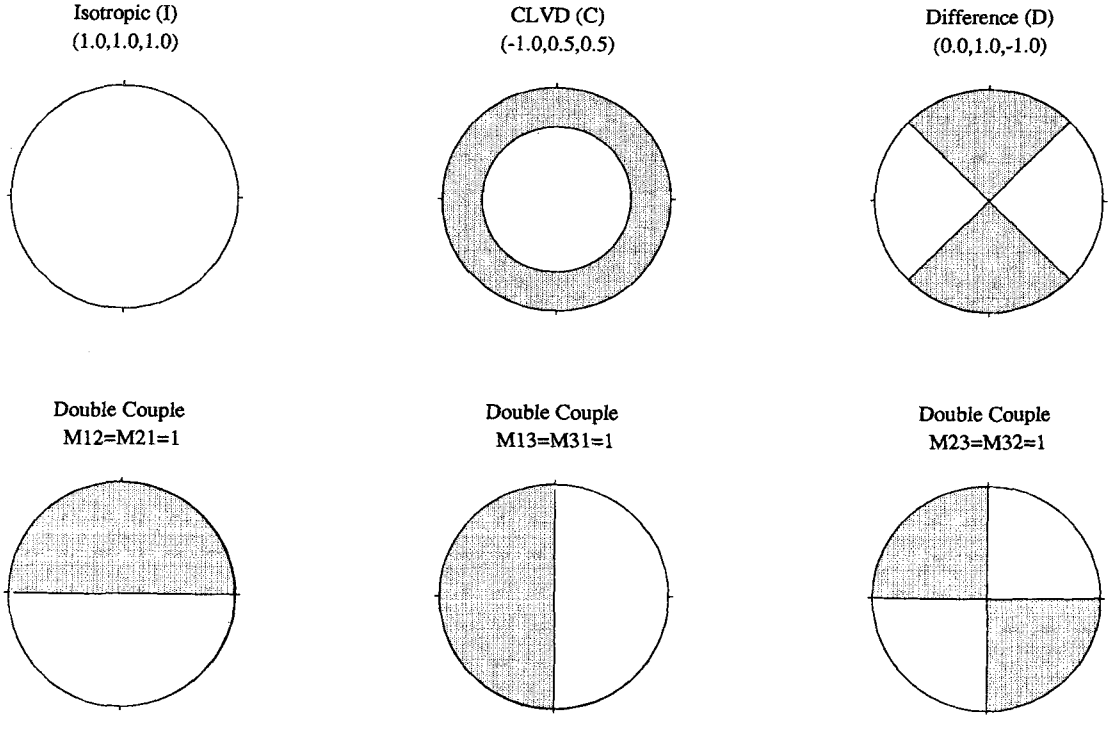

Figure 1. Notation for the six independent moment tensor elements used in this study.

The purpose of this paper is to discuss the observability of the isotropic component of the moment tensor in general. By performing many controlled tests for moment tensor inversion with synthetic data, we demonstrate that different data sets give different observabilities for the isotropic component; we show that it is possible to constrain the isotropic component of deep earthquakes using certain data sets. These theoretical results have been substantiated by Kawakatsu (1991) and Hara, Kuge & Kawakatsu (1995, 1996), who showed that there was no significant isotropic component in the moment tensors of the deep earthquakes they studied.

EXCITATION BY A MOMENT TENSOR

Table 1 summarizes the excitation of *P, SV, SH,* Rayleigh and Love waves due to each element of a moment tensor. For a general moment tensor, it is useful to introduce a new set of parameters for the diagonal components; we define the isotropic (I), vertical CLVD (C) (Knopoff & Randall 1970) and difference (D) components of the moment tensor by

$$I \equiv \frac{1}{3}(M_{\theta\theta} + M_{\phi\phi} + M_{rr}), \tag{1}$$

$$C \equiv \frac{1}{3}(M_{\theta\theta} + M_{\phi\phi} - 2M_{rr}) = (DV_{\theta\theta} + DV_{\phi\phi}), \tag{2}$$

$$D \equiv \frac{1}{2}(M_{\theta\theta} - M_{\phi\phi}) = \frac{1}{2}(DV_{\theta\theta} - DV_{\phi\phi}), \tag{3}$$

where

$$DV_{ij} \equiv M_{ij} - I\delta_{ij} \tag{4}$$

is the deviatoric part of the moment tensor.

Inspection of Table 1 shows that the reorganization of the diagonal components ($M_{\theta\theta}, M_{\phi\phi}, M_{rr}$) into ($I, C, D$) gives the most nearly independent set of parameters (Fig. 1). Since neither I nor C excites waves with azimuthal dependence, these two components are difficult to resolve independently using only data observed at the Earth's surface. Furthermore, Mendiguren & Aki (1978) pointed out that the ratio of $N_R^{(1)}$ and $S_R^{(1)}$, which are the excitation coefficients for I and C respectively (*cf.* Kanamori & Given 1981), is a weak function of seismic frequency (especially for shallow earthquakes, Fig. 2), and that it is therefore very difficult to distinguish these components by analysing long-period surface waves or narrow-band low-frequency normal-mode data. The only way to observe the isotropic component independently seems to be to analyse many body waves which radiate from the source with different take-off angles and which are first radiated as P waves at the source.

The portion of seismograms between the first P-wave arrival and just before the arrival of the first surface wave train contains many different body-wave phases, including *P, PcP, PP, PS,* and others. Synthetic seismograms of such long-period (10–22 mHz) body waves of a deep earthquake indicate that the isotropic and the vertical CLVD components excite these waves quite differently (Fig. 3a), whereas they excite surface waves similarly (Fig. 3b). It should thus be possible to distinguish these two components by analysing long-period body waves.

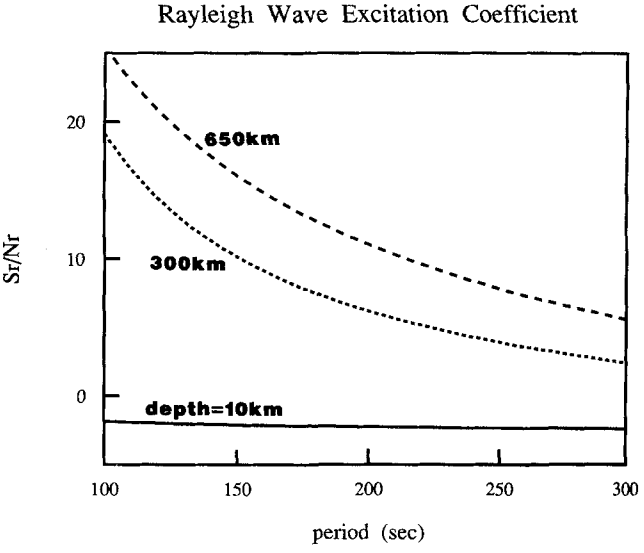

Figure 2. The ratio of the excitation coefficients of Rayleigh waves for I ($N_R^{(1)}$) and C ($S_R^{(1)}$) as a function of period.

OBSERVABILITY OF THE ISOTROPIC COMPONENT

Defining the vector $\boldsymbol{m} = (I, C, D, M_{r\theta}, M_{r\phi}, M_{\theta\phi})$, we can write the displacement of the ith record $u_i(x, t)$ as

$$u_i(x, t) = \sum_{j=1}^{6} \psi_{ij}(x, t) m_j, \tag{5}$$

where $\psi_{ij}(x, t)$ can be theoretically calculated for known source and receiver locations.

A least-squares moment tensor (i.e. $\boldsymbol{m}$) inversion using seismic waveforms can be given by the following normal equation:

$$\boldsymbol{A} \cdot \boldsymbol{m} = \boldsymbol{b}, \tag{6}$$

where the elements of the normal-equation matrix are

$$A_{ij} = \sum_k \int_{t_{k_1}}^{t_{k_2}} \psi_{ki}\psi_{kj}\, dt, \tag{7}$$

with t_{k_1} and t_{k_2} being the beginning and the end times for the kth seismogram; the elements of the vector $\boldsymbol{b}$ are

$$b_i = \sum_k \int_{t_{k_1}}^{t_{k_2}} u_k\psi_{ki}\, dt \tag{8}$$

(e.g. Dziewonski & Woodhouse 1983b).

The observability of each element of a moment tensor for a given set of seismograms can be estimated from the unscaled covariance matrix $\boldsymbol{A}^{-1}$. For the purpose of later discussion, we define the relative standard deviation of each element σ_i by

$$\hat{\sigma}_i = \sqrt{A_{ii}^{-1}}/\sigma_1, \tag{9}$$

where $\sigma_i = \sqrt{A_{ii}^{-1}}$, and the correlation matrix $\boldsymbol{X}$ is given by

$$X_{ij} = A_{ij}^{-1}/\sigma_i\sigma_j. \tag{10}$$

Since the normal-equation matrix $\boldsymbol{A}$ can be calculated if the epicentral location and station distribution are known, the correlation matrix $\boldsymbol{X}$ and the relative standard deviation $\hat{\sigma}$ can be obtained. Thus, some of the basic statistical properties of

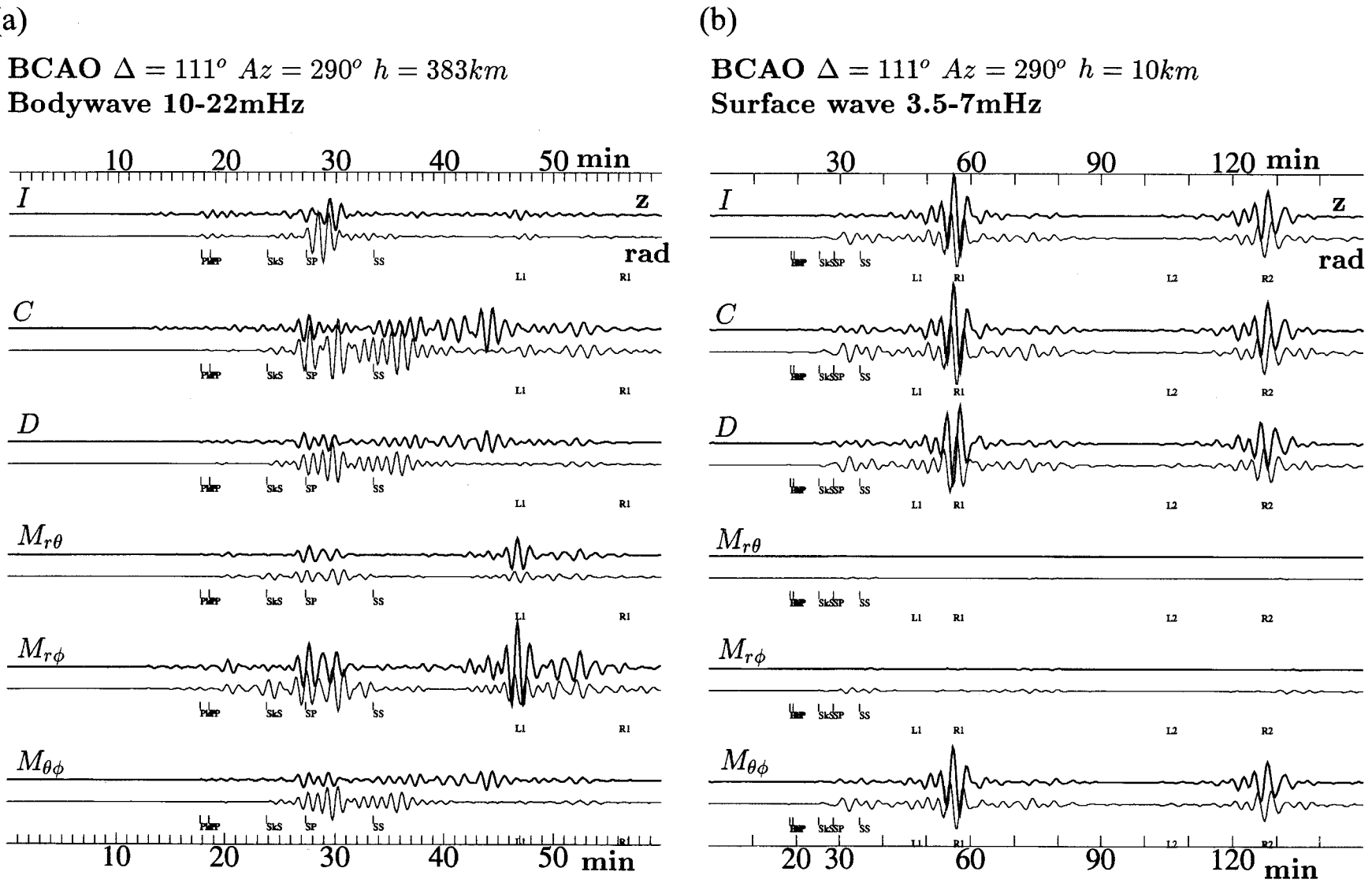

Figure 3. Synthetic seismograms of long-period body waves for a deep earthquake (a), and long-period surface waves for a shallow earthquake (b). The earthquake is located at the hypocentre of the south of Honshu event (event 7 in Table 2) and the station is BCAO (azimuth = 290°, Δ = 111°; see Fig. 8). The waveforms are calculated by a summation of normal modes and filtered with a passband of (a) 10–22 mHz and (b) 3.5–7 mHz. For each pair of seismograms, the top trace is for the vertical component and the bottom trace is for the radial component. Six pairs of seismograms are shown for six moment tensor elements. Note that the body-wave waveforms of the deep earthquake for the isotropic component and *C* component are quite different (a), but this is not the case for long-period surface waves (b). The expected arrival times of some major phases are also indicated.

the inversion for the moment tensor can be theoretically known without having actual observed waveforms; we can thus perform some numerical experiments for idealized source and station distributions to investigate the observability of each element of the moment tensor.

Here we consider the two different kinds of data sets shown in Fig. 3: long-period (10–22 mHz) body-wave waveforms between *P*-wave and Love-wave arrivals; and long-period (3.5–7 mHz) surface-wave waveforms which contain the first two major wave trains (e.g. R1 and R2). Both are the type of seismograms used by the Harvard group for their centroid moment tensor (CMT) inversion (e.g. Dziewonski, Chou & Woodhouse 1981; Dziewonski & Woodhouse 1983a). Synthetic seismograms are calculated by summing all the normal modes within a given frequency band, and thus can be considered exact for the assumed Earth structure [1066A of GD75 plus the five-layer Q^{-1} model of Masters & Gilbert (1983)].

Fig. 3 show the synthetic seismograms excited by each moment tensor element. For each pair of seismograms, the top and bottom traces are the vertical and the radial components, respectively. The transverse components are not shown because the I component does not excite them. In order for each moment tensor component to be resolved using these types of waveforms, the waveforms must look significantly different from those excited by other components. Fig. 3(b) shows long-period surface waves for a shallow event. The similarity of the waveforms corresponding to the I and C components immediately suggests the difficulty of resolving these two components using this type of data. The small amplitude of $M_{r\theta}$ and $M_{r\phi}$ also indicates the difficulty of resolving these components for shallow earthquakes using surface waves (e.g. Kanamori & Given 1981). Fig. 3(a) is for long-period body waves of a deep event. Waveforms corresponding to the I and C components are significantly different, suggesting the possibility of resolving the isotropic component of deep earthquakes using long-period body waves.

CONTROLLED TESTS

In order to investigate whether long-period body-wave waveforms can be used to resolve the isotropic component, we calculate the relative standard deviation (9) and correlation matrix (10) for an idealized station distribution: the epicentre is located at the north pole and stations are located at 30° intervals in both co-latitude and longitude, giving a total of 61 stations. Three-component seismograms are computed for each station by the summation of normal modes. As long-period body-wave data, we use waveforms from the origin time until just before the Love-wave arrival times. As long-period surface-wave data, we use waveforms starting from just before the arrival time of the so-called X-phase surface waves (overtone surface waves, Tanimoto 1987) to 9000 s after the origin time; with this time window, each seismogram contains at least one first minor-arc surface wave (i.e. G1 or R1). Figs 4(a) and (b) show the results for a shallow (10 km) event, and Figs 4(c) and (d) show the results for a deep (600 km) event. In each figure, eigen solutions of the normal-equation matrix A are shown on the left. The vertical lines in each row give the contribution of the moment tensor elements for each eigenvector, whose relative eigenvalue is given on the left, with the corresponding focal mechanism on the right. Those mechanisms (i.e. eigenvectors) that have larger eigenvalues are better resolved. Vertical lines at the top-right indicate the sizes of the relative standard deviations $\hat{\sigma}$, and the correlation matrix X is shown on the bottom-right.

The correlation matrix for a shallow event using long-period surface-wave data (Fig. 4a) indicates an almost complete correlation between the I and C components, while other combinations of two components are uncorrelated. This means that it is impossible to distinguish between the I and C components of a shallow earthquake using these data. There actually are only three significant eigenvectors that can be resolved, because of the well-known difficulty of constraining $M_{r\theta}$ and $M_{r\phi}$ components for shallow events (Kanamori & Given 1981). The eigenvector with the smallest eigenvalue ($0.754I - 0.657C$) is actually very close to the vertical vector dipole M_{rr}. So, in this case it is not the isotropic component but the vertical dipole component that cannot be resolved. The use of long-period body waves does not improve the situation much for a shallow event; although the difficulty of observing $M_{r\theta}$ and $M_{r\phi}$ components is now reduced (see the relative standard deviations), there is still a strong correlation between the I and C components [correlation coefficient (X_{IC}) of -0.85, Fig. 4b]. Again the eigenvector with the smallest eigenvalue ($0.607I - 0.795C$) is close to the pure vertical vector dipole.

For a deep event , the situation is slightly better, even using long-period surface-wave data (Fig. 4c). The correlation coefficient between the I and C components is now reduced to 0.52, but there is still a strong correlation. The use of long-period body waves, however, improves the situation dramatically; now the correlation between the I and C components is very small (-0.03). The eigenvector with the smallest eigenvalue is an almost pure isotropic component, and the relative standard deviations show a large value for the I component. Both these factors suggest the relative difficulty of observing this component. At least, however, the inversion result will not be biased much by the presence of the C component, which, as will be shown later, is often quite large for deep earthquakes. This confirms the earlier suggestion that it may be possible to resolve the isotropic component of deep earthquakes by analysing long-period body waves.

Fig. 5 summarizes the depth dependence of the correlation coefficient between the I and C components in this controlled test. These coefficients are obtained for the assumed earth structure and for the idealized station coverage. In the actual inversion for the moment tensor, many different kinds of noise exist. If the noise is white, the inverted moment tensor will not suffer much from the large correlation between the I and C components, although the reliability can be small (i.e. the standard deviations can be large). In reality, mislocation of the hypocentre, inaccuracy in the earth model, and uneven station distribution all act as sources of correlated (non-white) noise and could severely bias the resulting solution if some of the components are strongly correlated. This could result in serious errors when estimating the isotropic component of deep earthquakes, because the C components can often be very large for down-dip compressional earthquakes, which are very common for deep events occurring within subducting slabs. It is, therefore, essential that the correlation coefficient between the I and C components be small in order to resolve the isotropic component of deep earthquakes. Fig. 5 indicates that this condition may be satisfied for deep events (at a depth of 350 km, $X_{IC} = -0.20$) using long-period body waves.

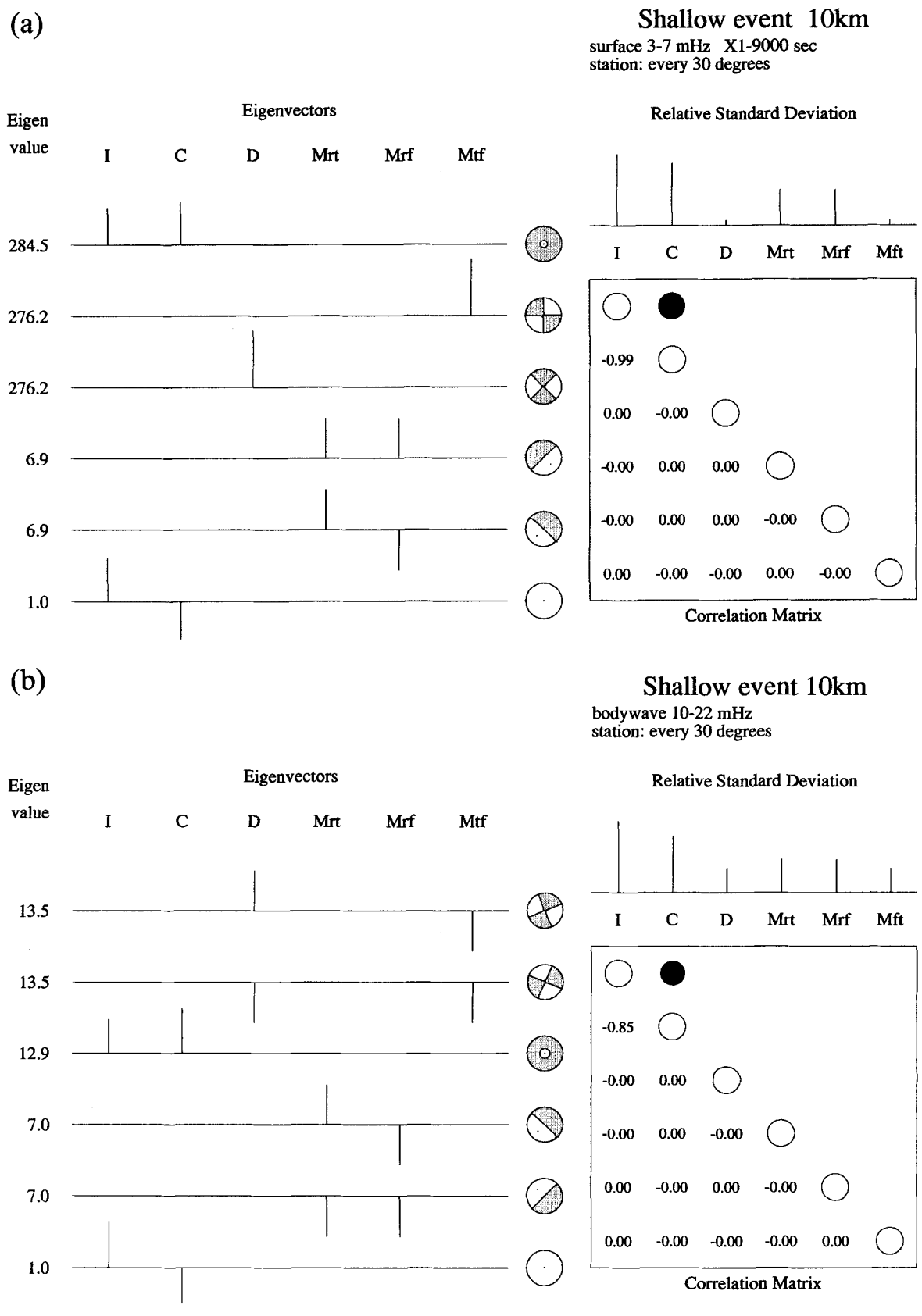

Figure 4. Result of the controlled tests using surface-wave and body-wave data for events at depths of 10 and 600 km. In each figure, eigensolutions of the normal-equation matrix $\boldsymbol{A}$ are shown on the left: vertical lines in each row give the contributions of moment tensor elements for each eigenvector, whose relative eigenvalue is given on the left, with the corresponding focal mechanism on the right; the relative standard deviation $\hat{\sigma}$ and the correlation matrix $\boldsymbol{X}$ are shown on the right. The size of circle is proportional to the magnitude of the correlation coefficient.

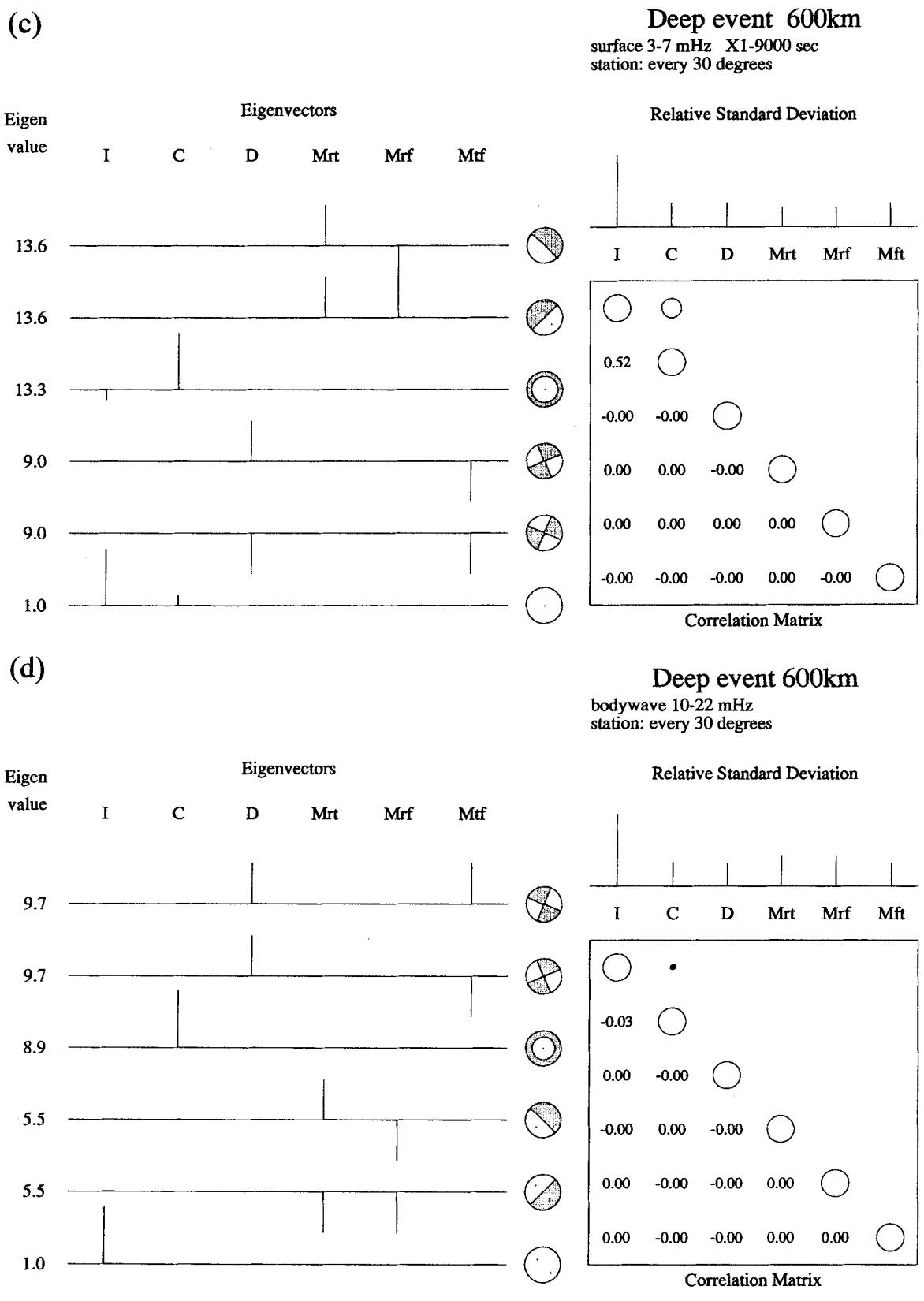

Figure 4. (*Continued.*)

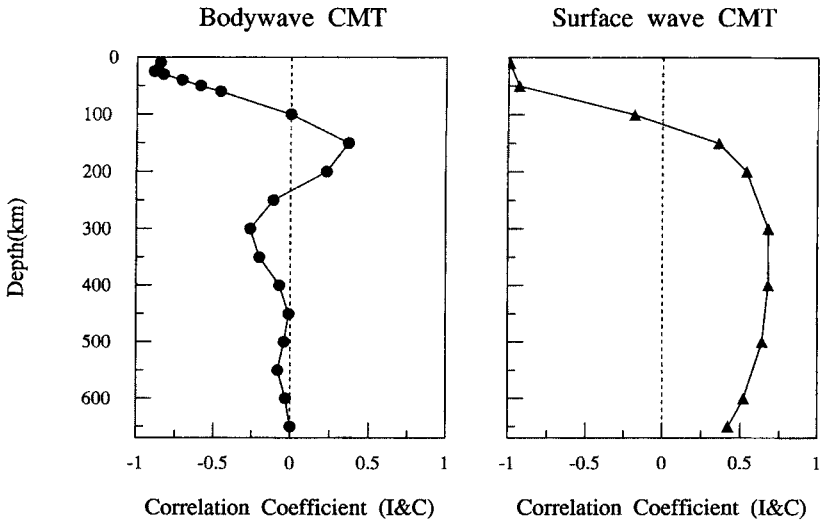

Figure 5. The correlation coefficient between I and C (X_{IC}) is given as a function of source depth. The results for body-wave and surface-wave inversions are shown on the left and on the right, respectively.

FULL CMT INVERSION OF DEEP EARTHQUAKES

Following the controlled test in the previous section, we perform CMT inversions of deep earthquakes using long-period body waves. The method is essentially the same as that developed by Dziewonski *et al.* (1981); we perform iterative inversion in the time domain. We use GDSN long-period seismograms as data for all events, and we also use IDA and GEOSCOPE data when they are available. We deconvolve the instrument response for each seismogram and bandpass filter them between 10 and 22 mHz. The sampling interval of data is 6 s, and each seismogram is weighted by the inverse of its root mean square.

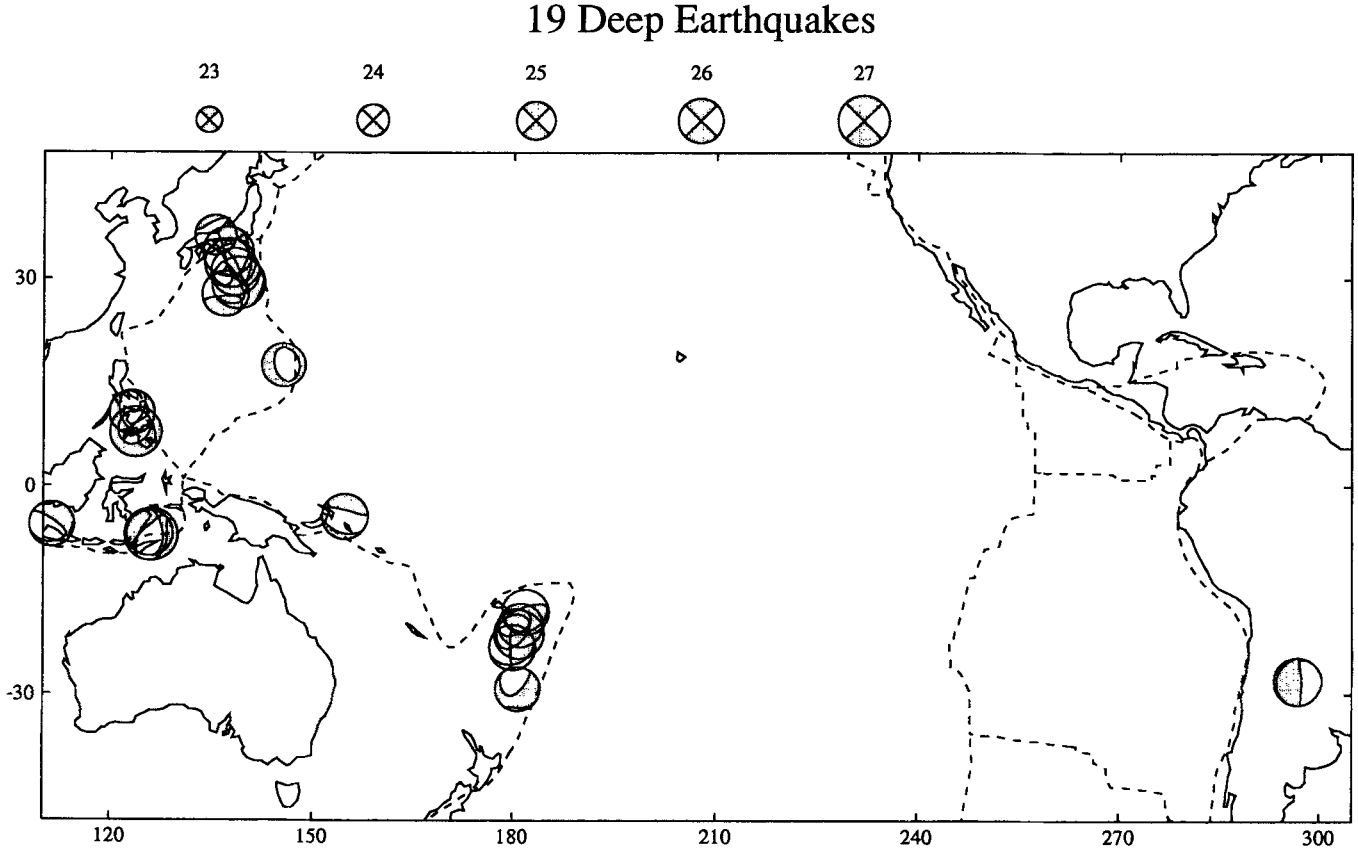

Figure 6. The locations of 19 deep earthquakes (Table 2) studied here are shown with the lower-hemisphere plot of the corresponding Harvard CMT solutions.

Error estimate

The statistical properties of CMT solutions are estimated after convergence is obtained. To compute the scaled covariance matrix of the moment tensor, we use the number of degrees of freedom on the frequency domain instead of the number of data points in the time domain. This is because the real number of degrees of freedom should be less than the number of data points when the data are bandpass-filtered. For the ith seismogram, the number of degrees of freedom is estimated by

$$frd_i = frd_0 \frac{nt_i}{N_{\mathrm{FFT}}}, \tag{11}$$

where nt is the number of points, and N_{FFT} is the number of points used for the FFT. The parameter frd_0 is the number of pass-band points in the frequency domain and is equal to N_{FFT} when an all-pass filter is used for the inversion. The total number of degrees of freedom is estimated by

$$frd_{\mathrm{tot}} = \sum_i frd_i - N_{\mathrm{par}}, \tag{12}$$

where N_{par} is the number of parameters determined by the inversion. Then the covariance matrix is scaled by frd_{tot}, instead of by $\Sigma_i nt_i$.

Application for 19 deep earthquakes

We performed systematic body-wave CMT inversions for two sets of deep earthquakes that occurred between 1978 and 1986. The first set consists of nine events whose reported Harvard moment tensor solutions exhibit large deviatoric non-double-couple components ($\varepsilon > 0.15$, Nos 1–9 in Table 2). The second set consists of all the events during this period whose seismic moments are greater than 10^{19} N m (Nos 10–19 in Table 2). The first group is chosen because the large non-double-couple components of these events may indicate somewhat unusual focal processes. The epicentral locations are shown in Fig. 6.

Fig. 7 summarizes the inversion results for the 1984 January 1, south of Honshu event. At the top left, an equal-area projection of the lower hemisphere of the focal mechanism is shown. At the top right, the relative amplitude of our moment tensor elements is plotted, as are the corresponding Harvard CMT solutions. The correlation matrix and the eigen solutions are shown in a similar fashion to those in Fig. 4. This event is well suited for a test of the method, because it has good station coverage (Fig. 8) and because it has a well-documented large deviatoric non-double-couple moment tensor (Ekström *et al.* 1986; Kuge & Kawakatsu 1990) which may indicate a somewhat unusual source mechanism. The

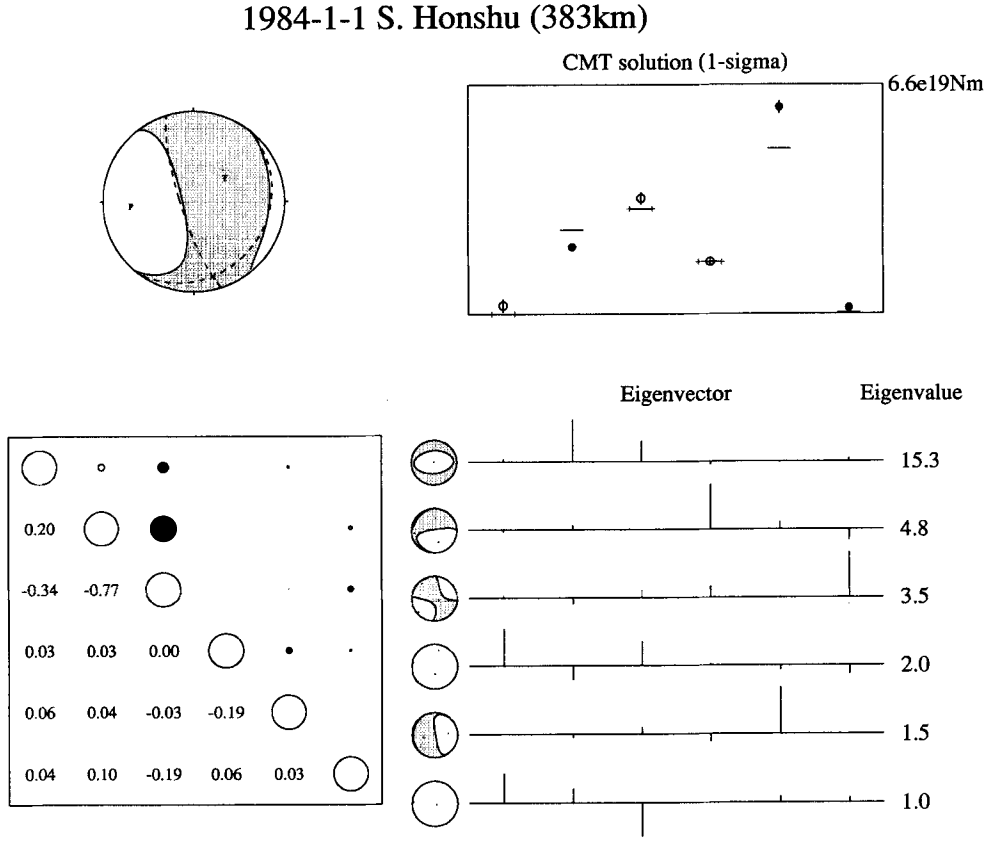

Figure 7. Example of the CMT inversion for the south of Honshu earthquake (1984 January 1, depth = 383 km). Upper-left: equal-area projection (lower hemisphere) of the CMT solution—note the large non-double-couple component. Upper-right: relative amplitude of each component of a moment tensor. The vertical error bars indicate one standard deviation. Open and closed circles indicate positive and negative values, respectively. The horizontal bars show the corresponding Harvard CMT solution (where there are plus marks at both ends, the value is positive, otherwise it is negative). Note that the isotropic component is almost zero. Lower-left: corresponding correlation matrix. Lower-right: eigensolutions of the normal-equation matrix (see caption for Fig. 4).

Table 2. 19 deep earthquakes.

No.	date						latitude	longitude	depth*	moment*	ϵ*	τ*
1	78	3	7	2	48	39.4	31.96	137.61	434.4	5.38×10^{19}	-0.17	9.0
2	80	3	31	7	32	31.8	35.45	135.47	367.1	2.14×10^{18}	0.27	3.0
3	81	9	28	17	56	19.6	-29.31	180.77	309.1	7.57×10^{18}	-0.17	5.0
4	81	10	7	3	2	14.7	-20.61	181.20	624.6	7.07×10^{18}	-0.21	5.0
5	82	1	4	6	5	1.3	18.03	145.63	595.2	6.69×10^{18}	-0.17	3.0
6	82	7	4	1	20	8.2	27.91	136.92	551.8	1.25×10^{19}	0.17	10.0
7	84	1	1	9	3	37.5	33.40	137.32	383.6	6.05×10^{19}	-0.20	14.0
8	84	3	5	3	33	51.2	8.14	123.77	644.1	9.29×10^{19}	-0.35	15.0
9	86	6	16	10	48	27.6	-21.90	180.96	564.8	4.49×10^{19}	-0.20	12.6
10	80	3	29	4	7	41.7	-4.60	154.88	480.4	1.45×10^{19}	0.15	5.0
11	81	4	28	21	14	48.2	-23.72	179.98	553.3	1.30×10^{19}	-0.00	6.0
12	81	9	4	11	14	15.3	11.05	123.21	635.7	1.02×10^{19}	0.00	7.0
13	82	6	22	4	18	40.5	-7.36	126.12	473.4	1.77×10^{20}	0.07	15.5
14	82	10	7	7	15	56.9	-7.16	125.91	521.1	1.33×10^{19}	0.06	7.4
15	83	12	21	12	5	6.0	-28.23	296.80	599.9	2.70×10^{19}	-0.02	10.5
16	84	3	6	2	17	21.1	29.36	138.87	446.0	1.44×10^{20}	-0.12	18.3
17	84	4	24	4	11	30.9	30.79	138.37	394.8	2.72×10^{19}	-0.04	11.1
18	84	7	9	23	19	3.3	-5.85	111.29	531.4	1.15×10^{19}	-0.01	7.9
19	84	11	17	13	45	49.1	-18.74	181.91	471.5	1.45×10^{19}	0.01	8.7

* Harvard CMT.

The non-double couple (deviatoric) parameter ε is defined by $\varepsilon = -\lambda_2/\max(|\lambda_1|, |\lambda_3|)$, where $\lambda_1, \lambda_2, \lambda_3 (\lambda_1 \geq \lambda_2 \geq \lambda_3)$ are eigenvalues of the deviatoric moment tensor DV_{ij} (Giardini 1983). $\varepsilon = 0$ for a double couple mechanism, and takes a value between -0.5 and 0.5 for a deviatoric moment tensor.

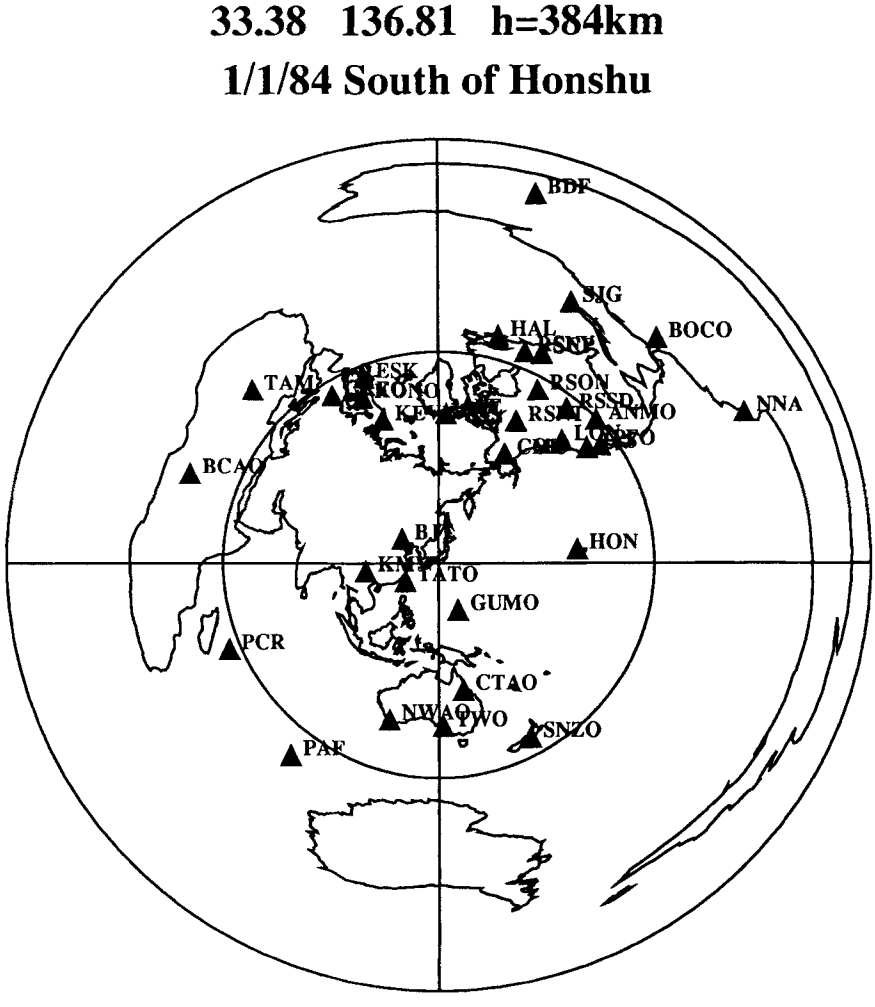

Figure 8. Station distribution for the south of Honshu earthquake.

isotropic component is essentially zero and the correlation matrix indicates that the isotropic component is well resolved. The eigenvectors that have significant isotropic components have the smallest eigenvalues. This suggests that it is still relatively difficult to observe the isotropic component even using long-period body-wave data. This is because the isotropic component is less efficient in exciting seismic waves in general, but the solution at least will not be biased by the presence of the vertical CLVD component.

Figs 9 and A1 and Table 3 show the results for the rest of the 18 deep earthquakes. The absolute values of the correlation coefficients between I and C are smaller than 0.21, and for most of the more recent events they are smaller than 0.10. We may, therefore expect the isotropic components to be reasonably well resolved for these deep earthquakes. As can be seen in Figs 9 and A1, the I components are very small in absolute values and for most events they are the smallest. The two-standard-deviation error bars always cut through the zero value and their presence is statistically insignificant within the 95 per cent confidence interval. Fig. 10 shows the size of the isotropic component as a function of depth for all 19 events. The isotropic components are given as a percentage of the deviatoric seismic moment, and the horizontal bars show the standard deviation. For all 19 deep earthquakes studied, the isotropic components are smaller than 10 per cent of the deviatoric seismic moments. Two-standard-deviation error bars always cut through the zero isotropic value. There appears to be no systematic difference between events with large non-double-couple components and events without them. The sign of the isotropic component shows no systematic pattern, while an implosive phase change should always result in a negative isotropic component. These observations led Kawakatsu (1991) to conclude that no significant isotropic component exists in the moment tensor of deep earthquakes.

DISCUSSION

Although the results presented above suggest that there is no significant isotropic component for deep earthquakes for frequencies between 10 and 22 mHz, they do not completely rule out the possibility of the existence of an isotropic component at lower frequencies, if the isotropic component contains most of its energy below 10 mHz and/or if its source time function is significantly different from that of the other components. If this is the case, as was suggested by DG74 and GD75, then time-domain CMT inversion using band-limited body-wave waveforms may not be sensitive to the isotropic component. In this case, we might have to use normal-mode data at the longest periods.

Controlled test for normal-mode data

Controlled tests similar to those performed above for body-wave and surface-wave CMT inversions can be easily performed for normal-mode moment tensor inversion. We locate the source and receivers in the same way as we did for the above CMT inversions, and calculate correlation matrices for the moment tensor components. As for the waveforms, we use

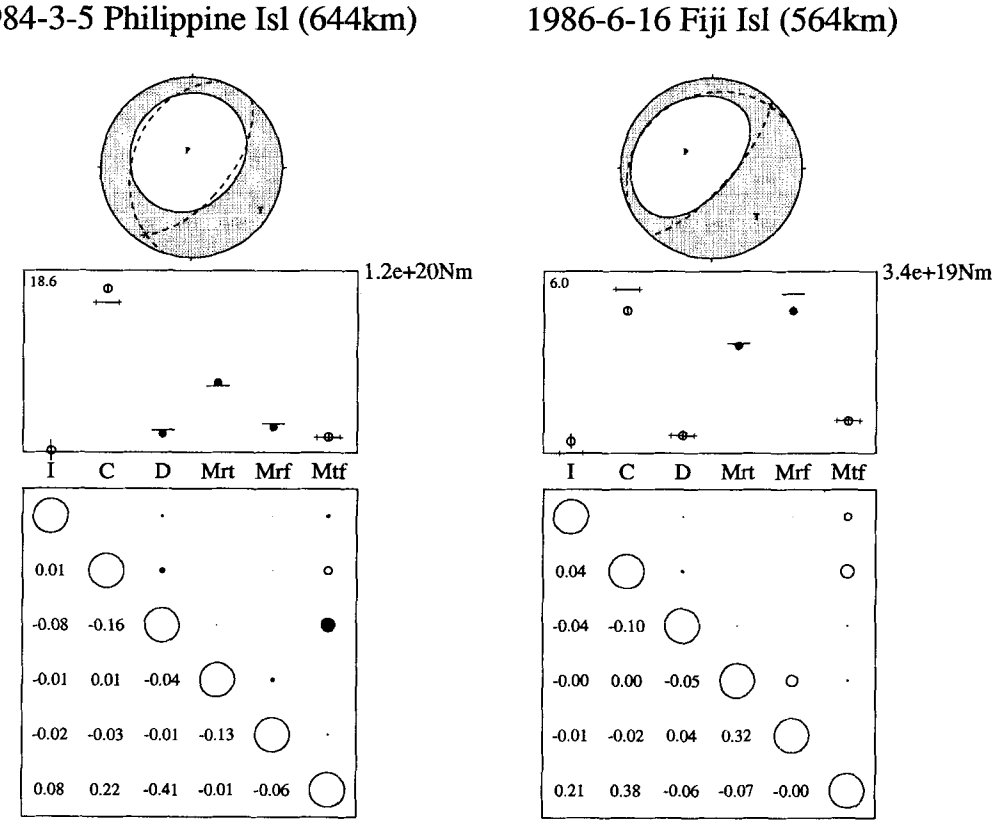

Figure 9. CMT solutions of events 8 and 9 in Table 2. Focal mechanism, moment tensor solution and correlation matrix of each earthquake are shown (see captions to Figs 4 and 7 for details). The condition number (the ratio of the largest to the smallest eigenvalues) of the normal-equation matrix is shown at the upper-left corner of the middle box. CMT solutions for the remaining 16 deep earthquakes are shown in Fig. A1.

Table 3. CMT solutions.

No	*lat*	*lon*	*depth*	Δt	I	C	D	$M_{r\theta}$	$M_{r\phi}$	$M_{\theta\phi}$	M_o	EX	α	ϵ
	Δlat	Δlon	$\Delta depth$		σ_I	σ_C	σ_D	$\sigma_{r\theta}$	$\sigma_{r\phi}$	$\sigma_{\theta\phi}$		×10	%	
1	31.25	137.40	438.5	13.7	0.21	-1.34	1.56	1.21	-3.47	0.09	4.12	19	4.8	-0.15
	-0.71	-0.21	4.1		0.36	0.15	0.22	0.17	0.28	0.21				
2	35.01	135.36	367.6	6.7	-0.16	0.61	0.83	-1.34	0.26	0.69	1.80	18	-8.0	0.16
	-0.44	-0.11	0.5		0.16	0.07	0.11	0.10	0.07	0.09				
3	-29.10	180.83	312.0	3.4	0.19	1.42	-2.52	-4.49	-2.83	1.22	6.12	18	3.0	-0.04
	0.21	0.06	2.9		0.22	0.12	0.22	0.17	0.17	0.17				
4	-20.28	181.01	620.9	6.7	0.17	3.73	1.76	-3.79	-3.53	1.03	6.43	18	2.5	-0.06
	0.33	-0.19	-3.7		0.35	0.15	0.17	0.19	0.17	0.18				
5	17.69	145.50	607.1	3.3	0.51	5.76	-1.50	-0.23	1.72	-1.08	5.52	18	8.4	-0.17
	-0.34	-0.13	11.9		0.45	0.20	0.15	0.17	0.16	0.17				
6	27.79	136.56	546.6	3.0	0.02	0.27	0.45	-1.17	-0.16	-0.37	1.32	19	1.4	0.15
	-0.12	-0.36	-5.2		0.04	0.02	0.03	0.03	0.02	0.03				
7	33.33	137.02	383.9	9.7	0.24	-1.91	3.31	1.50	-5.91	-0.16	6.94	19	3.0	-0.24
	-0.07	-0.30	0.3		0.19	0.10	0.18	0.11	0.18	0.12				
8	8.20	123.74	644.7	9.6	0.12	10.69	-1.22	-4.56	-1.66	1.02	9.84	19	1.0	-0.37
	0.06	-0.03	0.6		0.69	0.31	0.19	0.25	0.24	0.24				
9	-21.47	180.97	561.1	10.0	0.22	2.68	0.34	-2.03	-2.68	0.61	4.09	19	5.0	-0.18
	0.43	0.01	-3.7		0.14	0.07	0.09	0.08	0.09	0.09				
10	-4.73	154.65	464.2	7.2	-0.06	0.86	0.21	0.90	0.01	-0.46	1.27	19	-4.8	-0.06
	-0.13	-0.23	9.1		0.12	0.05	0.07	0.07	0.06	0.08				
11	-23.45	179.76	546.3	8.5	0.03	-0.20	0.22	0.15	-1.08	-0.49	1.22	19	2.4	-0.01
	0.27	-0.22	-7.0		0.05	0.02	0.04	0.03	0.05	0.04				
12	9.91	124.31	635.1	65.6	0.77	6.24	-6.14	-3.02	-0.28	1.79	8.81	18	8.1	0.15
	-1.14	1.10	-0.6		0.61	0.28	0.38	0.26	0.30	0.22				
13	-6.71	125.93	472.3	16.5	-0.04	0.98	-0.68	0.84	0.19	0.78	1.59	20	-2.1	0.06
	0.65	-0.19	-1.1		0.07	0.04	0.05	0.05	0.04	0.05				
14	-6.78	125.72	511.3	5.4	-0.03	0.71	-0.58	0.50	0.08	0.19	1.01	19	-2.7	-0.04
	0.38	-0.19	-9.8		0.05	0.03	0.04	0.03	0.03	0.03				
15	-27.83	297.05	596.4	7.0	-0.02	-0.88	0.69	0.02	1.44	-0.26	1.78	19	-0.9	-0.14
	0.40	0.25	-3.5		0.08	0.04	0.06	0.04	0.07	0.06				
16	29.52	138.77	445.4	8.0	-0.02	0.24	0.49	0.54	-1.58	-0.30	1.76	20	-1.1	-0.14
	0.16	-0.10	-0.6		0.06	0.02	0.04	0.03	0.05	0.03				
17	30.68	138.22	400.7	4.0	-0.10	1.05	0.69	0.36	-2.03	-1.34	2.71	19	-3.8	-0.04
	-0.11	-0.15	5.9		0.09	0.04	0.06	0.06	0.07	0.06				
18	-5.95	111.28	538.7	4.8	0.35	3.16	3.44	4.26	-4.08	-0.98	7.42	18	4.6	0.04
	-0.09	-0.01	7.3		0.41	0.17	0.22	0.25	0.21	0.23				
19	-18.37	181.98	470.4	8.5	-0.09	-0.68	-0.24	-0.98	-0.38	-0.22	1.25	19	-7.0	0.01
	0.37	0.07	-1.1		0.05	0.02	0.03	0.04	0.02	0.03				

The isotropic component parameter α is the ratio of the isotropic component and the seismic moment of the 'best double couple' (Dziewonski & Woodhouse 1983a).

the theoretical complex spectrum between 0 and 10 mHz for the same earth model as used above. We use a sampling interval of 0.005 mHz and divide the 10 mHz long spectrum into 10 frequency windows and calculate correlation matrices for each window.

Fig. 11 shows the correlation coefficients of the I and C components for earthquakes located at depths of 50, 300, and 600 km. For the shallow earthquake, I and C are strongly negatively correlated; especially at the lowest frequencies they are almost perfectly anti-correlated and thus it is almost impossible to resolve the isotropic component using low-frequency normal-mode data. For the deep earthquake (600 km), the situation is quite different. The correlation coefficients for frequencies above 6 mHz (167 s) are reasonably small, suggesting the possibility of resolving the isotropic component in this frequency range, although the effect of the Earth's lateral heterogeneity may severely restrict practical applications. In the frequency range between 2 and 6 mHz (500–167 s), I and C are strongly positively correlated, suggesting that resolving the isotropic component will be difficult in this frequency range. Below this frequency range, the sign of the correlation coefficients changes from positive to negative, and in the lowest interval (0–1 mHz) the I and C components are completely anti-correlated.

Isotropic component of the Columbian earthquake

DG74 and GD75 inferred the existence of a significant slow implosive isotropic component, which preceded the main rupture by about 80 s, for two large deep earthquakes. Since then, many researchers have discussed the validity of the inferred isotropic source, but none of these studies appears to be conclusive.

Fig. 12 reproduces GD75's source spectrum for the diagonal components of the moment tensor for the Columbian earthquake. We first point out that the frequency range for which they reported the significant isotropic component is between 2.4 and 6.4 mHz (note that in their figure the frequency is given by the angular frequency: 0.015–0.04 rad s^{-1}); this is exactly the frequency range in which we expect a strong positive correlation between I and C, as discussed above (Fig. 11). Fig. 13 shows their moment tensor solutions for the two deep earthquakes in our notation. For both earthquakes, the C component dominates the solutions. Considering the

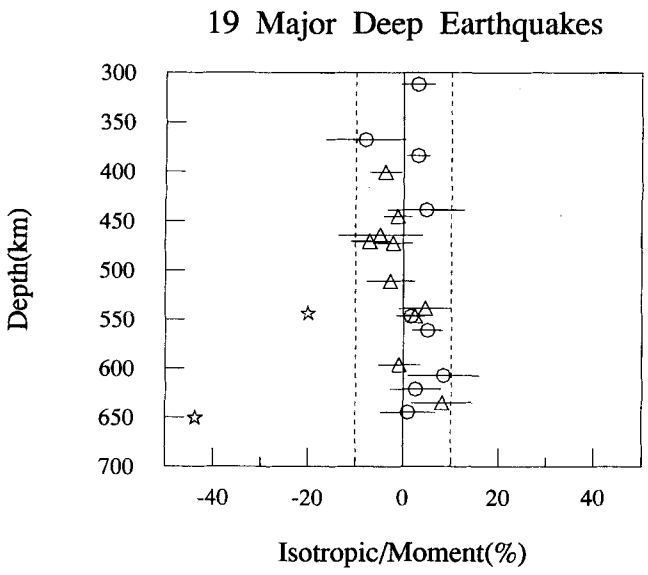

Figure 10. Depth distribution of the isotropic components of all 19 deep earthquakes. The horizontal axis shows the relative size of the isotropic component to the deviatoric seismic moment in per cent. Positive and negative values correspond to explosive and implosive isotropic sources, respectively. A deviatoric seismic moment is the average of the absolute values of the largest and the smallest eigenvalues of a deviatoric moment tensor, $DV_{ij} = M_{ij} - I\delta_{ij}$. The circles are for the nine events with large deviatoric non-double-couple components, and the triangles are for the 10 events with seismic moments over 10^{19} N m. The horizontal error bars indicate one standard deviation. The vertical broken lines indicate ± 10 per cent isotropic values, and all points are within this range. There also appears to be no systematic pattern and no difference between the two sets of deep earthquakes. Stars depict the isotropic components of two deep earthquakes studied by Dziewonski & Gilbert (1974).

large correlation coefficient between I and C, it is very likely that the I component is contaminated by the large C component in their solutions; the error on the centroid locations and the effect of the lateral heterogeneities, which were not considered in the DG papers, might have biased their estimate of the I component severely.

Based on the analysis presented in this paper and the result of Hara *et al.* (1995, 1996), we see no evidence of a significant isotropic component for deep earthquakes at any frequency. It seems highly unlikely that only the two events studied by Dziewonski & Gilbert would have happened to have a significant isotropic component. We thus conjecture that their conclusion has no sound basis, and that the large isotropic components they reported are due to the bias introduced by the presence of the large C components of these two deep earthquakes.

The possibility of constraining the isotropic component of deep earthquakes at lower frequencies

One of the most important findings in Fig. 11 is the change of the sign of the correlation coefficient at the lowest frequencies. For an event at a depth of 600 km, the change occurs somewhere between 1 and 3 mHz. This suggests that it may be possible to constrain the isotropic component of deep earthquakes by analysing normal-mode data in this frequency range, assuming that the frequency dependence of the moment tensor can be neglected. It is advantageous to analyse normal modes in the lowest frequency range, because the effect of asphericity of the Earth (i.e. rotation, ellipticity, and lateral heterogeneity) can be easily incorporated in the analysis (e.g. Hara *et al.* 1995). The only drawback is that only very large earthquakes can excite the low-frequency modes effectively.

The above fact and the occurrence of a gigantic deep

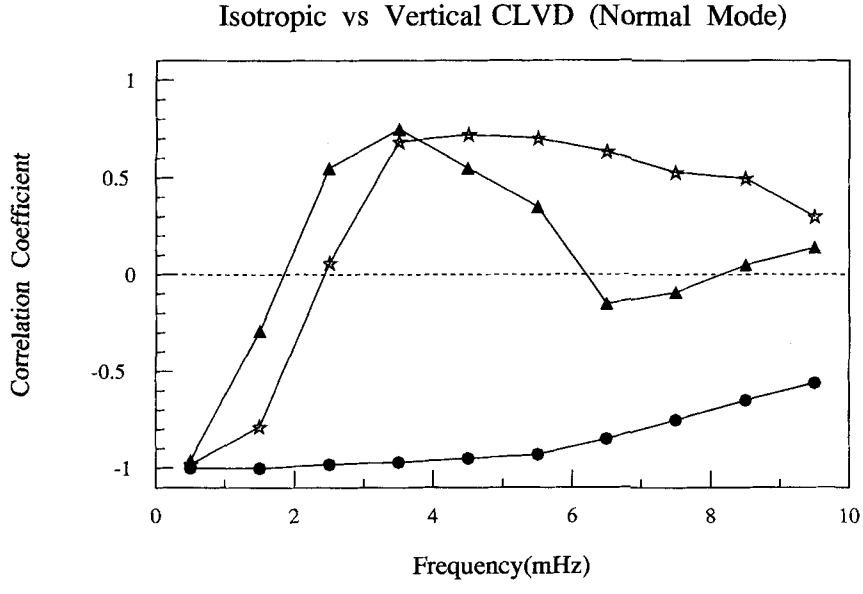

Figure 11. Result of the controlled test using normal-mode data. The correlation coefficients of I and C are shown as a function of frequency. For each 1 mHz wide frequency window, the moment tensor is assumed to be constant. Circles, stars and triangles correspond to the coefficients of earthquakes at depths of 50, 300, and 600 km, respectively.

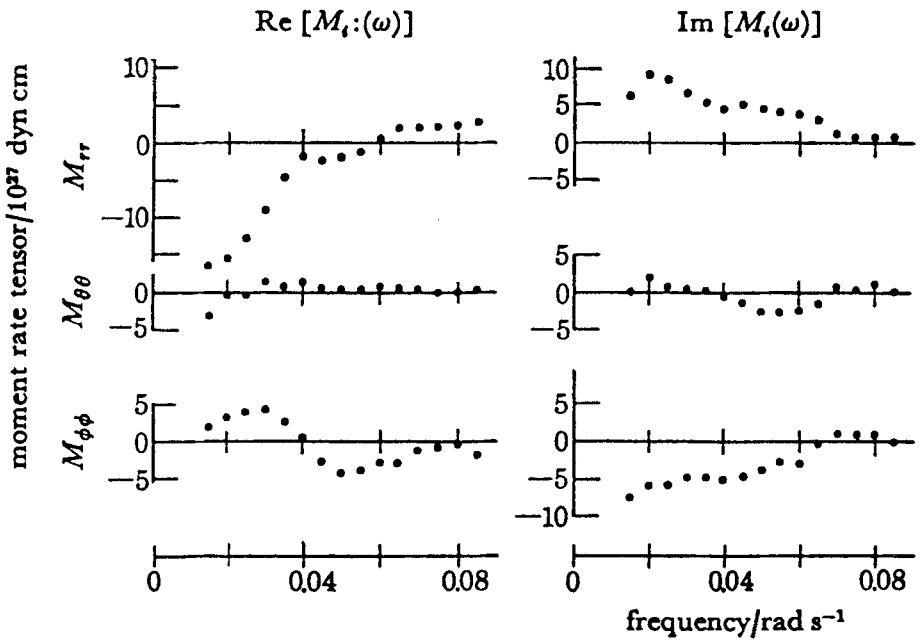

Figure 12. Complex spectrum of the diagonal components of the moment tensor of the Columbian deep earthquake obtained by inverting normal-mode data (after Gilbert & Dziewonski 1975). Note that a large isotropic component is obtained between 0.015 and 0.04 rad s^{-1} (~2.4–6.4 mHz), where the resolution is very bad (Fig. 11).

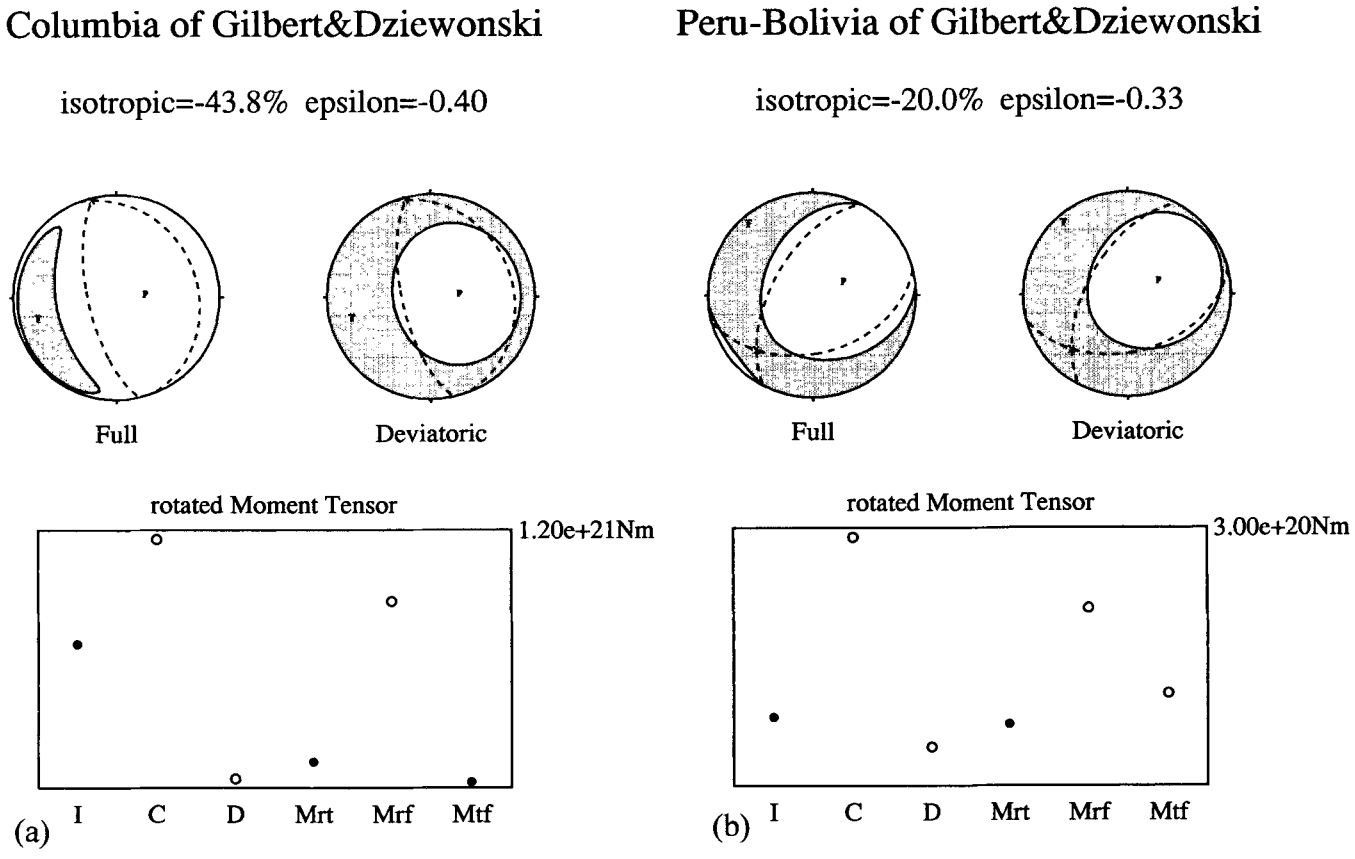

Figure 13. Full moment tensor solutions of DG papers for (a) Columbia and (b) Peru–Bolivia earthquakes. In each figure, the lower hemispheres of the focal spheres of the full and deviatoric moment tensors are shown at the top; at the bottom, the relative amplitude of each moment tensor element is given. Note the presence of the large *C* components for both earthquakes.

earthquake beneath Bolivia on 1995 June 9 (origin time: 00:33:13.2 UT; location: 13.737°S, 67.414°W; depth: 641 km; M_W: 8.2, after USGS) enabled Hara *et al.* (1995) for the first time to estimate reliably the full moment tensor, including the isotropic component, at the lowest frequencies (1–2 mHz). Fig. 14 shows the solution of Hara *et al.* (1995) which exhibits no significant isotropic component. Their analysis confirmed that the *I* and *C* components can be independently determined for this event using nomal-mode data.

CONCLUSION

The observability of the isotropic component of a general moment tensor is investigated by carefully examining its resolvability from the other components. The main conclusions of the paper are summarized as follows.

(1) The portion of the seismograms between the first *P*-wave arrival and just before the arrival of the first surface wave train can be used to constrain the isotropic component of deep earthquakes.

(2) Application of CMT inversion using this data set for major deep earthquakes revealed that there is no significant isotropic component for deep earthquakes.

(3) The isotropic component of deep earthquakes cannot be resolved independently from the vertical CLVD component by analysing the normal-mode data above 2 mHz that previous researchers used.

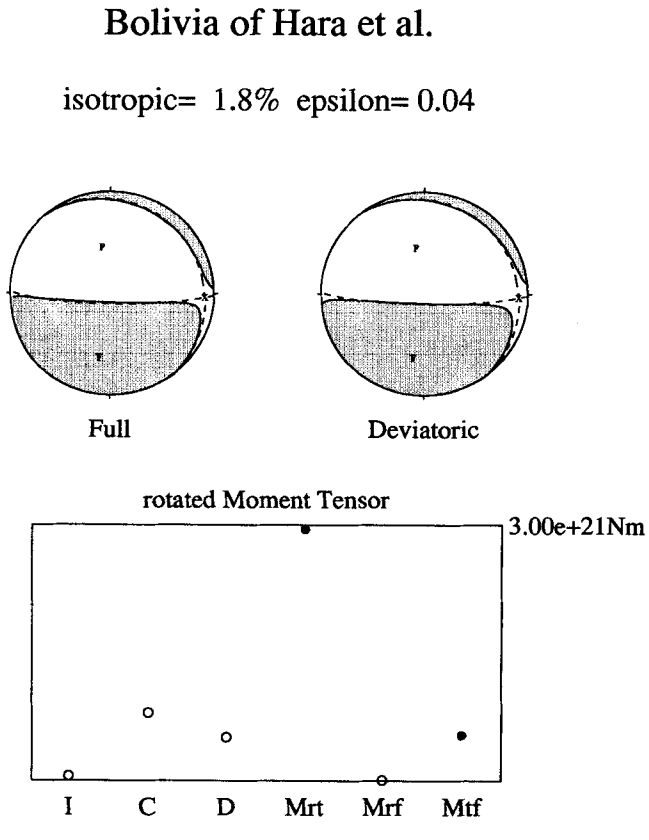

Figure 14. Similar plot to Fig. 13, but for the moment tensor of the 1994 Bolivia deep earthquake determined by Hara *et al.* (1995). The isotropic component is very small, and the full and deviatoric moment tensors are essentially the same.

(4) It should be possible to resolve the isotropic component of deep earthquakes using normal-mode data below 2 mHz.

ACKNOWLEDGMENTS

The author is grateful to Keiko Kuge and Toshihiko Hara for their encouragement to complete this paper, which was largely written several years ago. He also thanks Bob Geller for carefully reading the manuscript.

REFERENCES

Aki, K. & Richards, P.G., 1980. *Quantitative Seismology: Theory and Method,* Freeman, San Francisco, CA.

Backus, G. & Mulcahy, M., 1976. Moment tensors and other phenomenological descriptions of seismic sources—I. Continuous displacements, *Geophys. J. R. astr. Soc.,* **46,** 341–361.

Dziewonski, A.M. & Gilbert, F., 1974. Temporal variation of the seismic moment tensor and the evidence of precursive compression for two deep earthquakes, *Nature,* **247,** 185–188 (DG74).

Dziewonski, A.M. & Woodhouse, J.H., 1983a. An experiment in systematic study of global seismicity: centroid-moment tensor solutions for 201 moderate and large earthquakes in 1981, *J. geophys. Res.,* **88,** 3247–3271.

Dziewonski, A.M. & Woodhouse, J.H., 1983b. Studies of the seismic source using normal mode theory, in *Earthquakes: Observation, Theory and Interpretation,* pp. 45–137, ed. Kanamori, H.

Dziewonski, A.M., Chou, T.-A. & Woodhouse, J.H., 1981. Determination of earthquake source parameters from waveform data for studies of global and regional seismicity, *J. geophys. Res.,* **86,** 2825–2852.

Dziewonski, A.M., Franzen, J.E. & Woodhouse, J.H., 1984. Centroid-moment tensor solutions for January–March 1984, *Phys. Earth planet. Inter.,* **34,** 209–219.

Ekström, G., 1993. Rapid earthquake analysis at Harvard, *IRIS Newsletter,* **XII,** 4–6.

Ekström, G., Dziewonski, A.M. & Steim, J.M., 1986. Single station CMT; application to the Michoacan, Mexico, earthquake of September 19, 1985, *Geophys. Res. Lett.,* **13,** 173–176.

Geller, R.J., 1974. Evidence of precursive compression for two deep earthquakes, *Nature,* **252,** 28–29.

Giardini, D., 1983. Regional deviation of earthquake source mechanisms from the ⟨double-couple⟩ model, in *Proc. Enrico Fermi Int. Sch. Phys.,* **85,** pp. 345–353, eds Kanamori, H. & Boschi, E., North-Holland, Amsterdam.

Gilbert, F., 1970. Excitation of the normal modes of the Earth by earthquake sources, *Geophys. J. R. astr. Soc.,* **22,** 223–226.

Gilbert, F., 1973. Derivation of source parameters from low-frequency spectra, *Phil. Trans. R. Soc. Lond.,* A, **274,** 369–371.

Gilbert, F. & Dziewonski, A.M., 1975. An application of normal mode theory to the retrieval of structural parameters and source mechanisms from seismic spectra, *Phil. Trans. R. Soc. Lond.,* A, **278,** 187–269 (GD75).

Hart, R.S. & Kanamori, H., 1975. Search for compression before a deep earthquake, *Nature,* **253,** 333–336.

Hara, T., Kuge, K. & Kawakatsu, H., 1995. Determination of the isotropic component of the 1994 Bolivia deep earthquake, *Geophys. Res. Lett.,* **22,** 2265–2268.

Hara, T., Kuge, K. & Kawakatsu, H., 1996. Determination of the isotropic component of deep focus earthquakes by inversion of normal mode data, *Geophys. J. Int.,* submitted.

Kanmori, H. & Given, J.W., 1981. Use of long-period surface waves for rapid determination of earthquake source parameters, *Phys. Earth planet. Inter.,* **27,** 8–31.

Kanamori, H. & Given, J.W., 1982. Analysis of long-period seismic waves excited by the May 18, 1980, eruption of Mount St. Helens: A terrestrial monopole, *J. geophys. Res.,* **87,** 5422–5432.

Kawakatsu, H., 1989. Centroid single force inversion of seismic waves generated by landslides, *J. geophys. Res.*, **94,** 12 363–12 374.
Kawakatsu, H., 1991. Insignificant isotropic component in the moment tensor of deep earthquakes, *Nature,* **351,** 50–53.
Kawakatsu, H., 1995. Automated near-realtime CMT inversion, *Geophys. Res. Lett.,* **22,** 2569–2572.
Kennett, B.L.N. & Simons, R.S., 1976. An implosive precursor to the Colombia Earthquake 1970 July 31, *Geophys. J. R. astr. Soc.,* **44,** 471–482.
Knopoff, L. & Randall, M.J., 1970. The compensated linear-vector dipole: a possible mechanism for deep earthquakes, *J. geophys. Res.,* **75,** 4957–4963.
Kuge, K. & Kawakatsu, H., 1990. Analysis of a deep 'non-double-couple' earthquake using very broadband data, *Geophys. Res. Lett.,* **17,** 227–230.
Masters, G. & Gilbert, F., 1983. Attenuation in the Earth at low frequencies, *Phil. Trans. R. Soc. Lond.,* A, **308,** 479–522.
Mendiguren, J.A. & Aki, K., 1978. Source mechanism of the deep Colombian earthquake of 1970 July 31 from the free oscillation data, *Geophys. J. R. astr. Soc.,* **55,** 539–556.
Okal, E.A. & Geller, R.J., 1979. On the observability of isotropic seismic sources: The July 31, 1970 Colombian earthquake, *Phys. Earth planet. Inter.,* **18,** 176–196.
Riedesel, M.A., 1985. Seismic moment tensor recovery at low frequencies, *PhD thesis,* University of California at San Diego, CA.
Riedesel, M.A. & Jordan, T.H., 1989. Display and assessment of seismic moment tensors, *Bull. seism. Soc. Am.,* **79,** 85–100.
Silver, P.G. & Jordan, T.H., 1982. Optimal estimation of scalar seismic moment, *Geophys. J. R. astr. Soc.,* **70,** 755–787.
Sipkin, S., 1994. Rapid determination of global moment-tensor solutions, *Geophys. Res. Lett.,* **21,** 1667–1670.
Takei, Y. & Kumazawa, M., 1994. Why have the single force and torque been excluded from the seismic source model?, *Geophys. J. Int.,* **118,** 20–30.
Takei, Y. & Kumazawa, M., 1995. Phenomenological representation and kinematics of general seismic source including seismic vector modes, *Geophys. J. Int.,* **121,** 641–662.
Tanimoto, T., 1987. The three-dimensional shear wave structure in the mantle by overtone waveform inversion—I. Radial seismogram inversion, *Geophys. J. R. astr. Soc.,* **89,** 713–740.
Vasco, D.W. & Johnson, L.R., 1989. Inversion of waveforms for extreme source models with an application to the isotropic moment tensor component, *Geophys. J.,* **97,** 1–18.

APPENDIX A: CMT SOLUTIONS

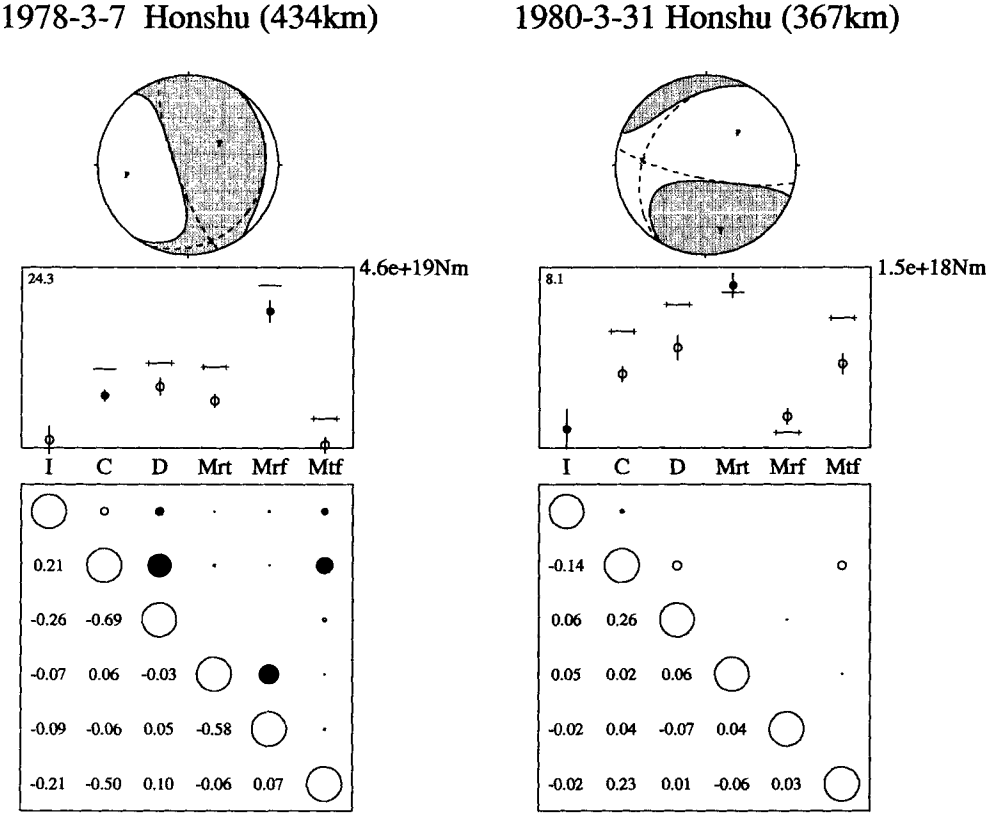

Figure A1. CMT solutions of the remaining 16 deep earthquakes (Table 2): focal mechanism, moment tensor solution and correlation matrix of each earthquake are shown (see captions of Figs 4, 7 and 9 for details).

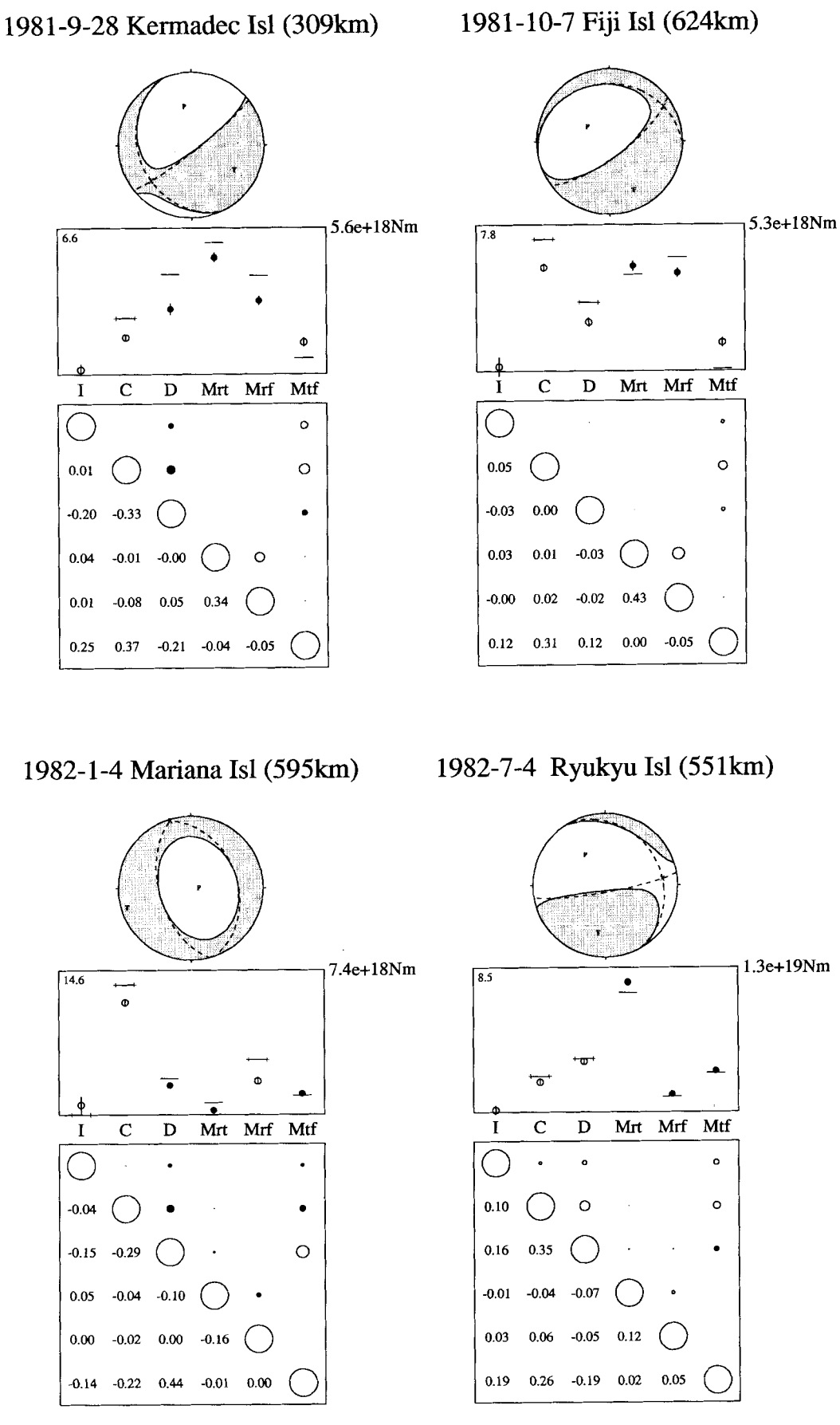

Figure A1. (*Continued.*)

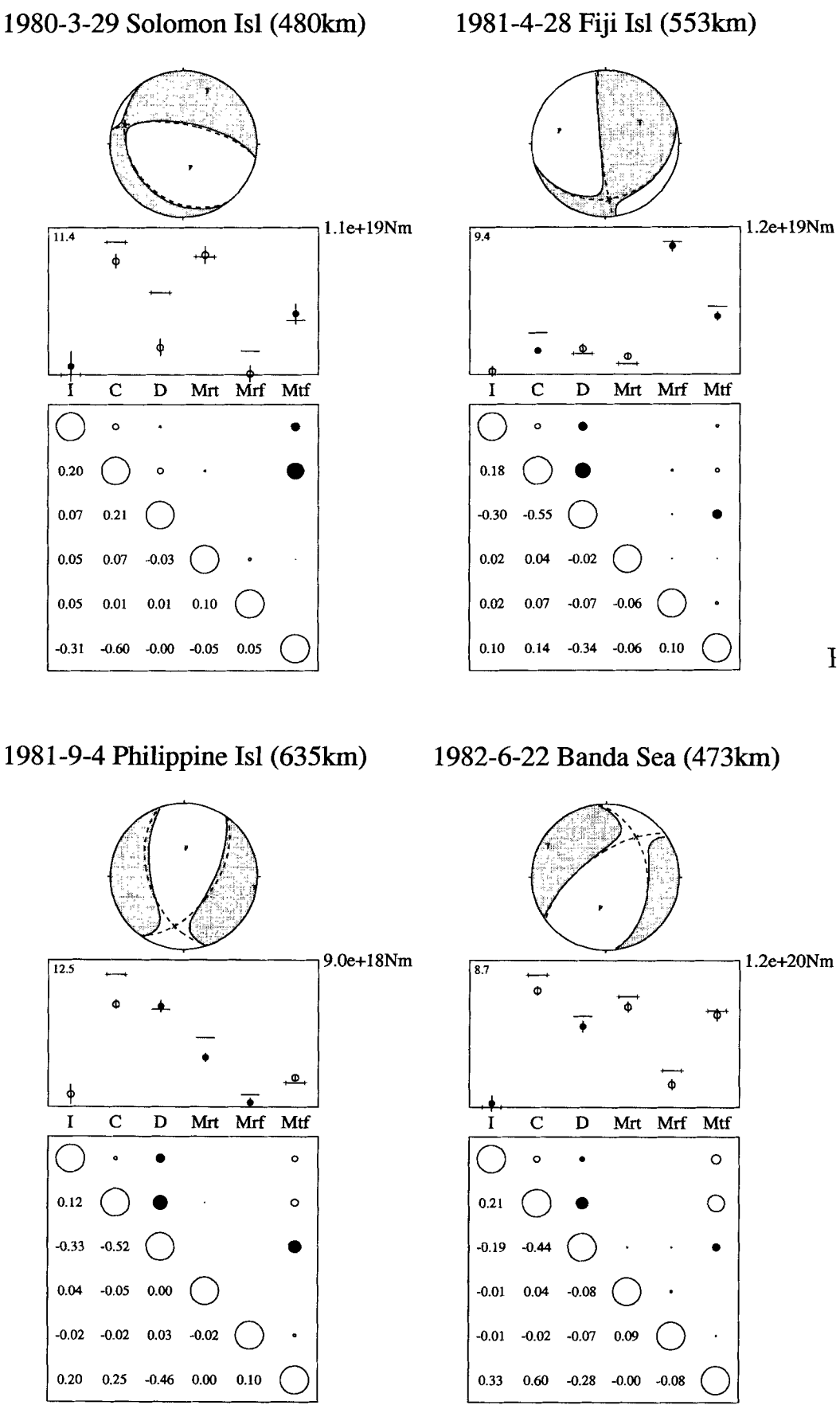

Figure A1. *(Continued.)*

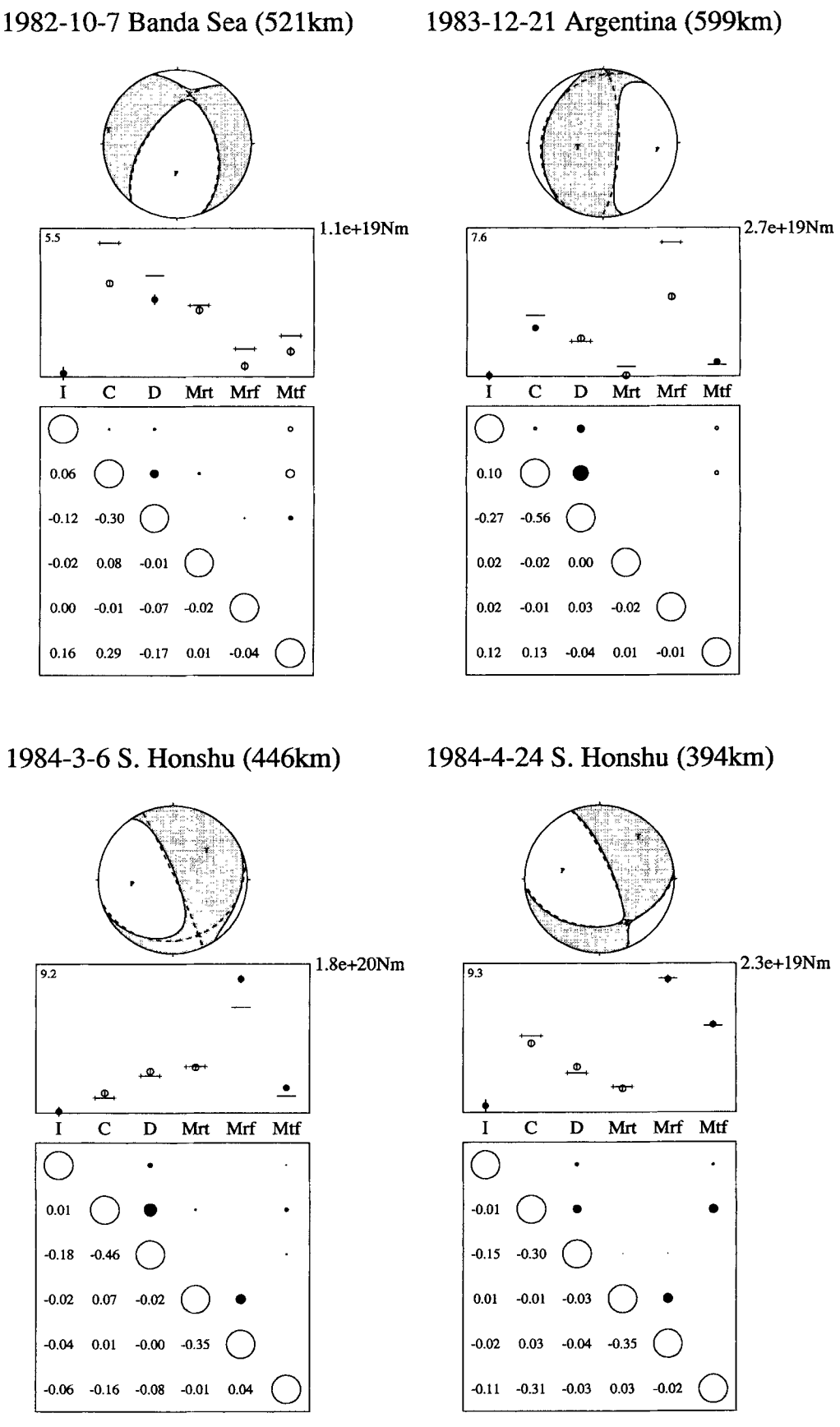

Figure A1. (*Continued.*)

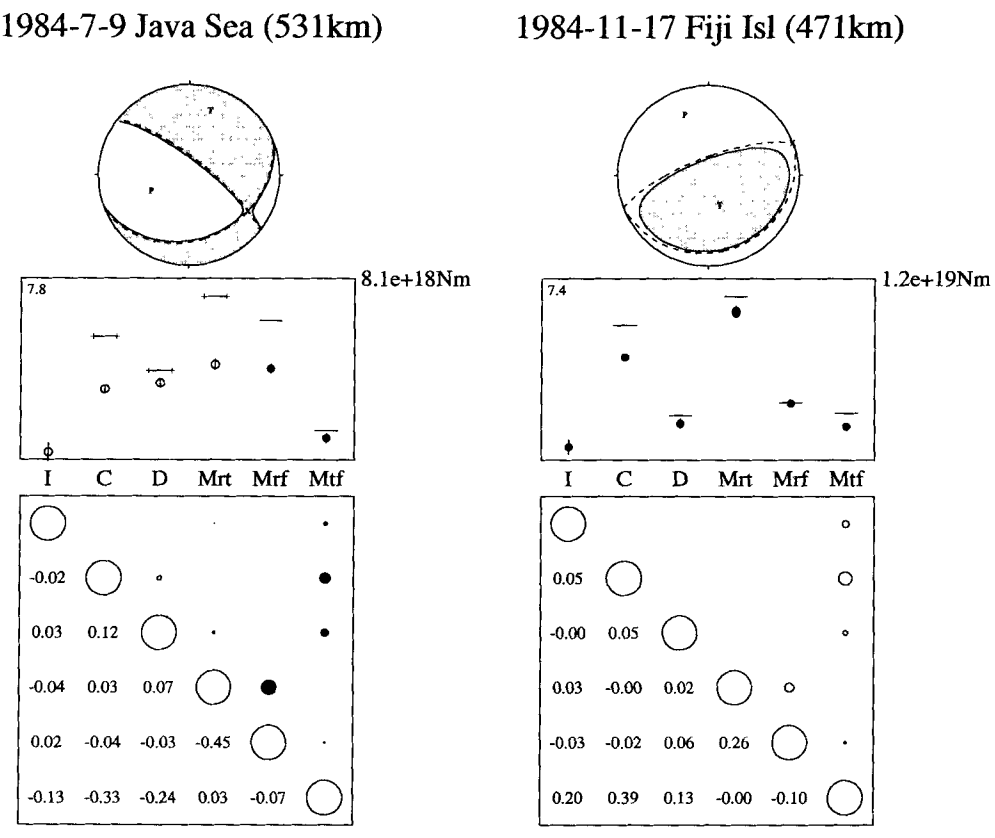

Figure A1. *(Continued.)*